CHAPTER II

THEORY AND LITERATURE REVIEWS

2.1 Supramolecular chemistry

The "supramolecular chemistry" or "chemistry of molecular assemblies and of the intermolecular bond" has been introduced by Jean-Marie Lehn in 1978 [31]. First of all, the concept of supramolecular chemistry was explained in term of the interaction of host and guest molecules via non-covalent bonds as shown in Figure 2.1.
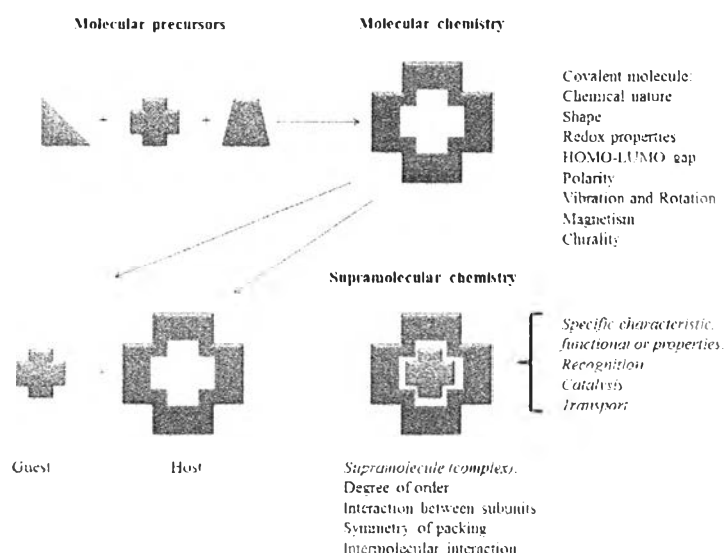

Figure 2.1 Comparison between the scope of molecular and supramolecular chemistry according to Lehn [31].

To obtain the supramolecular molecule, the molecules were interacted with not only additive but also cooperative interactions, involving hydrogen bonding, hydrophobic interactions and coordination and their chemistry of molecular information such as the storage of information at the molecular level and the structure feature were different from each individual component. Supramolecular chemistry is still a new scientific branch, which is moderately difficult to explain exactly what it encompasses. The overlapping phases in the development of supramolecular chemistry may be considered in three steps: (i) design and preorganization and implements information storage and processing (molecular recognition); (ii) design

and implements programming and programmed systems (concern about self-organization); (iii) emerging phase, it depend on the self-organization through selection [32].

Now a day, supramolecular chemistry has been used in many fields, not just using in host-guest system but also using in self-assembly and self-organization processes to prepare molecular recognitions, molecular devices and machines, and nanomaterials. The supramolecular interactions were widely used to operate the nanoparticle biological tasks, for example the preparation of nanoparticle-stabilized capsule with average diameter of 140±20 nm by non-covalent interactions, involving hydrogen bonding, hydrophobic and electrostatic interactions of proteins in drug molecules, AuNP and oil interior [33] as shown in Figure 2.2.
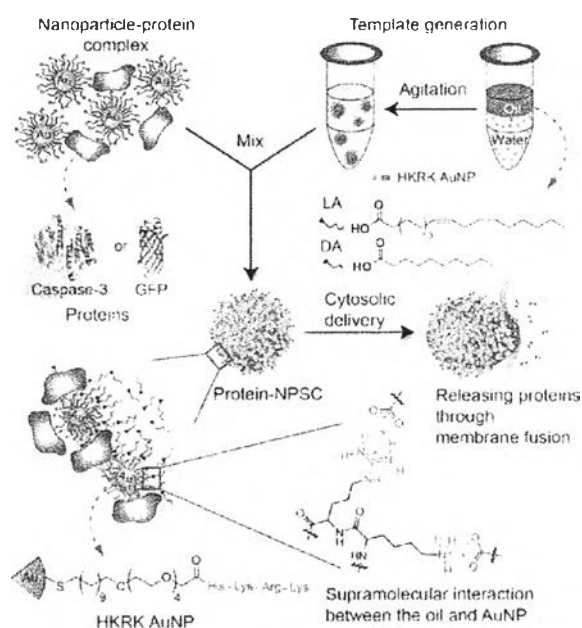

Figure 2.2 Design and preparation of nanoparticle-stabilized capsules (NPSCs) [33].

2.2 Nanoparticles

Nanoparticles [34] are microscopic particles with at least one dimensional size less than 100 nm. At present, nanoparticles were applied in many disciplines, particularly in biomedical, optical, and electronic fields systems. Nanoparticles are of great scientific interest as they are effectively a bridge between bulk materials and atomic or molecular structures. The properties of several conventional materials change upon forming of nanoparticles. Typically, nanoparticles have a greater surface

area per weight than the larger particles. Therefore, nanoparticles are more reactive than bulk molecules. Nanoparticles are applied in many fields. The following lists introduce many recent developments. [35]

1. Iron oxide and gadolinium nanoparticles were used to improve MRI images of cancer tumors.

2. Gold nanoparticles display many interesting electrical and optical properties. They can be as sensors such as using for detecting diseases as biosensors, improving the optical properties of materials, etc.

3. Magnetic nanoparticles that attach to cancer cells in the blood stream may allow the cancer cells to be removed before they establish new tumors.

4. Quantum Dots are crystalline nanoparticles that can be used to identify the location of cancer cells in the body.

5. Silver nanoparticles in fabric can kill bacteria making clothing odor-resistant.

2.3 Curcumin

Curcumin (diferuloylmethane) is a hydrophobic phenol molecule. Chemically, it has two o-methoxy phenols attached symmetrically via bis-α, β-unsaturated β-diketone linker that also induces keto–enol tautomerism [36]. Curcumin exhibits a predominant enol form in the low pH and the keto form is stable in alkaline media [7]. The keto-enol tautomeric equilibrium of curcumin is exemplified in Figure 2.3.
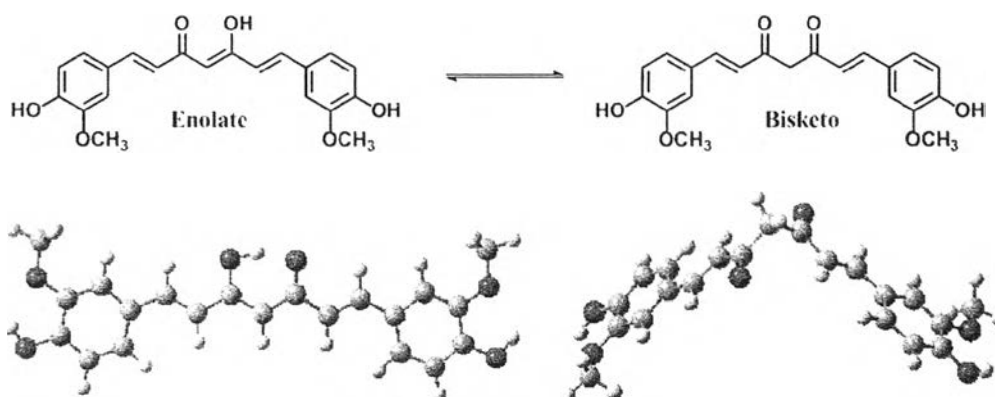

Figure 2.3 Chemical structures and optimized structures of curcumin in enol-keto tautomeric equilibrium [7, 37].

The geometry of enolic curcumin was characterized by DFT studies in both vacuum and solutions, the results showed that the enolic form (planar structure) was more stable than the diketo form (non-planar structure) [38]. The enolic form, which shows the planar structure with dihedral angle of 180° has a perfect resonance by electron circulated on the entire molecule resulting in the light absorption in visible spectral region. In contrast, the keto form shows the twistable structure, which is leading to an imperfect resonance.

Curcumin is a component of the root turmeric or *Curcuma longa L.*, which is widely used in pharmaceutical, food and cosmetics. Several studies found that curcumin exhibited the immense biological properties such as antioxidant properties, anti-inflammatory effect, anti-cancer and effective in preventing Alzheimer's disease [1-3]. Curcumin can kill a various tumor cell types such as PC-3 prostate cancer, SKOV-3, OVCAR-3 ovarian cancers, MCF-7 breast cancer, A549 lung cancer and HT29 colon cell lines by inducing apoptosis, the process of programmed cell death [39-42].

It is unclear that why curcumin selectively kills cancer cells and not normal cells. Nonetheless, many research showed interesting pathways to describe the possible mechanisms. First, the fluorescence image cells studies show that the cellular uptake of curcumin in cancer cells tend to be higher than in the normal cells [43]. Second, the glutathione levels in normal cells is higher than in cancer cells, thus it is possible that curcumin may be inactivated in normal cell by the conjugation of GSH and curcumin [44]. Third, the NF-kB is active in only many cancer cells, not normal cells, thus leading to an increasing of apoptotic process [45].

In vitro study, curcumin showed the anti-cancer activity in a wide variety of cancer cell lines. In contrast, *in vivo* study of curcumin showed the low anti-cancer activity, resulting in curcumin was generally water-insolubility and instability, causing the poor bioavailability in clinical trial [46,47]. The previous research showed rapidly degradation of curcumin in phosphate buffered saline (PBS) at pH 7.2 with half-life less than 10 min [48]. To increase the water-solubility and the bioavailability of curcumin, various materials have been used to encapsulate the curcumin.

2.4 Gadolinium ion [22,49]

Gd^{3+} is the lanthanide metal that widely used as a component of contrast agent for magnetic resonance image (MRI). The common commercial Gd (III) contrast agents based biocompatibility were shown in Figure 2.4. Gadolinium (III) was highly paramagnetic with seven unpaired electrons and a long electronic relaxation time, showing an excellent candidate as a relaxation agent. To reduce a toxicity of $[Gd(H_2O)_8]^{3+}$, it was conjugated with strong organic chelators before it was administered to patients. Current MRI agents require injection of gram quantities of Gd in order to obtain satisfactory contrast in the resulting image.
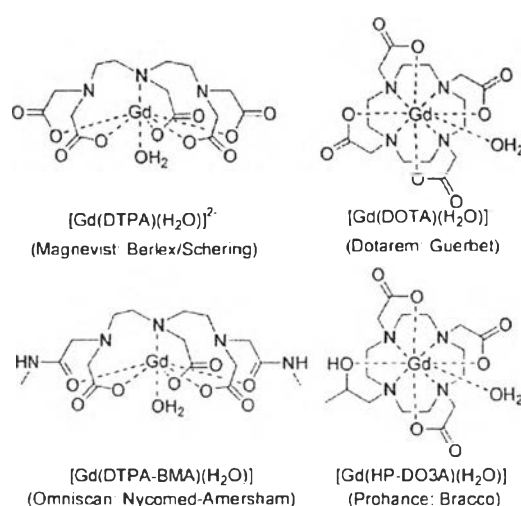

[Gd(DTPA)(H₂O)]²⁻
(Magnevist Berlex/Schering)

[Gd(DOTA)(H₂O)]
(Dotarem Guerbet)

[Gd(DTPA-BMA)(H₂O)]
(Omniscan Nycomed-Amersham)

[Gd(HP-DO3A)(H₂O)]
(Prohance: Bracco)

Figure 2.4 Common commercial Gd (III) contrast agents [49]

Table 2.1 Main luminescence transition of trivalent lanthanide aquo ions [22]

Ln	Excited state[a]	τ_{Rad}/ms[b]	End state[c]		Lumin. type[d]	λ/nm[e]	Emission color
Pr	$^1G_4$	n.a.	$^3H_6$	4-6	P	1300	NIR
	$^1D_2$	n.a.	$^3F_4$	2-4	P	890, 1060	NIR
	$^3P_0$	n.a.	^3H_J	4-6	F	525-680	Orange
Nd	$^4F_{3/2}$	0.42	^4I_J	9/2-15/2	F	1060	NIR
Sm	$^4G_{5/2}$	6.26	^6H_J	5/2-15/2	P	590	Orange
Eu	$^5D_0$	9.67	^7F_J	0-6	P	620	Red
Gd	$^6P_{7/2}$	10.9	$^8S_{7/2}$		P	312	UV
Tb	$^5D_4$	9.02	^7F_J	6-0	P	550	Green
Dy	$^4F_{9/2}$	1.85	^6H_J	15/2-5/2	P	570	Yellow-orange
Ho	$^5F_5$	n.a.	^5I_J	8-4	F	970, 1450	NIR
	$^5S_2$	0.37	^5I_J	8-4	F	540	Green
Er	$^4S_{3/2}$	0.66	^4I_J	15/2-9/2	F		
	$^4I_{13/2}$	n.a.	$^4I_{15/2}$		F	1530	NIR
Tm	$^1G_4$	n.a.	^3H_J	6-4	P		
Yb	$^2F_{5/2}$	1.2[f]	$^2F_{7/2}$		F	980	NIR

[a] Most luminescent excited states. [b] Radiative lifetime of the excited state for aquo ions, from ref. 17. Radiative lifetimes vary substantially from one compound to another. [c] Range of J-values indicated on the right hand side. [d] F: fluorescence; P: phosphorescence. [e] Approximate wavelength of most intense emission lines (or emission range). [f] For [Yb(dtpa)]²⁻, from ref. 16.

In generally, many lanthanide ions possessed fascinating optical properties, especially using in application of cellular imaging by luminescence of lanthanide ions, the electronic transition of trivalent lanthanide showed in Table 2.1. In the case of Gd^{3+}, the emission spectrum was occurred in the UV region. It was useful to use as the component of adaptive suparmolecular network to encapsulate dye molecule without the luminescence interference from lanthanide ions.

2.5 X-Ray Method

Since the discovery of X-rays in the late 19th century, several of X-ray techniques and methods are in use; E. D. Olsen could classify all methods as falling in one of three main categories: absorbtion, emission, and diffraction, but in this research, we will show just only two method;

2.5.1 X-ray absorption (XAS) [50,51]

X-ray absorption method is a commonly used technique to define the local geometric and/or electronic structure of matter. That is analogous to absorption methods in other regions of the electromagnetic spectrum. A beam of X-ray is usually performed at synchrotron radiation sources, which is passed though the sample, and the attenuation, or fraction of X-ray photons absorbed will be examined as a measure of the concentration of the absorbing substance. The X-ray method is helpful to measure not only in the thickness solid sample but also in the gas-phase and solution.

The absorption of X-ray follows Beer's law, which can be defined in term of

$$I = I_0 e^{-\mu x} \quad \ldots\ldots\ldots\ldots\ldots (2\text{-}1)$$

When; I_0 = incident intensity of X-ray

I = intensity of X-ray after passing though absorbing sample

x = *path length, cm*

μ = mass absorption coefficient, cm^2/g

The equation (2-1) can be shown in the new form

$$\mu x = ln(I_0/I_1) \quad \ldots\ldots\ldots\ldots\ldots (2\text{-}2)$$

When among increase the photon energy, I_0 and I_1 will be detected and calculated to the term of normalized absorption or μx, which calls the XAS spectra.
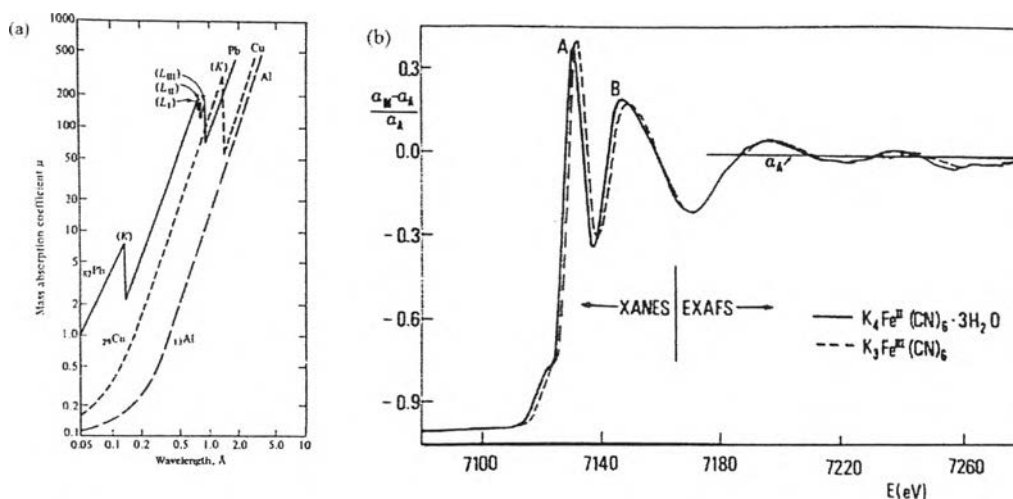
Figure 2.5 (a) Mass-absorption coefficients for lead, copper, and aluminum as a function of wavelength. (b) K-edge x-ray absorption spectra of iron in $K_3Fe(CN)_6$ and $K_4Fe(CN)_6$ [50,51].

The XAS spectra in a plot of mass-absorption coefficient (μ) and wavelength of each element were shown in Figure 2.5(a), sharp discontinuous peak called *absorption edges* are found. The spectra show that the probability of absorption enhances as the wavelength enhances, until the absorption edge is reached, when the sharp drop off occurs. At x-ray energies equal to or slightly greater than the absorption edge, there is a high probability that the x-ray will interact and eject electron in question, whereas when the x-ray energy is less (wavelength longer) than the absorption edge, the probability for ejection of that electron falls sharply.

X-ray absorption near-edge structure or XANES is absorption spectrum covers the range between the threshold and the point at which the extended x-ray absorption fine structure, EXAFS, begins, 5 eV above the edge to 150 eV as shown in Figure 2.5 (b). The XANES region will show the interaction of photoelectron with the surrounding atoms resulting in the original dominant in the XANES spectra. The normalized absorption spectra or XANES spectra are widely used to define the average oxidation state of the element in the sample. The XANES spectra of an unknown sample were monitored by the matching with known standards called Finger printing methods. Linear combination fitting of several different standard spectra from software analysis can provide the amount of each of the known standard spectra within an unknown sample.

The extended x-ray absorption fine spectra (EXAFES) are the fine structure in the high energy range (150-2000 eV). The simplifying single-scattering assumption leading to EXAFES spectra is examined in this region, which is a powerful tool to determine the atomic pair distribution such as the distance between a center atom to backscattering atom.

2.5.2 X-ray diffraction (XRD)

X-ray diffraction is widely used technique to determine such as crystal structure, composition of solid, particle size, evidence of decomposition, polymorphism, preferred orientation and dis-order [52].
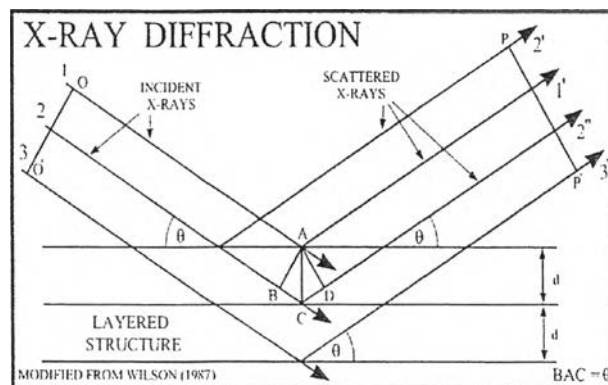
Figure 2.6 Diffraction of X-ray from a set of crystal planes [53]

The phenomenon of scattering occurs when primary radiation forces the electrons in the same frequency leading to the oscillation and emitting electromagnetic radiation in all direction. The sum of all scattered waves in a crystal plane will be reinforced traveling in certain direction (called diffracted) and out-of-phase or diminished, wavefronts in other direction as shown in Figure 2.6. The unique diffraction pattern of each crystalline substance produced a fingerprint of its atomic and molecular structure.

The conditions for diffraction are governed by Bragg's law

$$CB = BD = l$$

$n\lambda$ must be equal $2l$ for reinforcement, where n is an integer. In Figure 2.6, it can be written that

$$l = d\sin\theta$$

hence, $n\lambda = 2d\sin\theta$ .... (2-3)

2.6 Inductively Coupled Plasma-Atomic Emission Spectroscopy (ICP-AES)

Inductively Coupled Plasma-Atomic Emission Spectroscopy is type of emission spectroscopy technique, which is used to determine the trace metals at the ultratrace level on μl or μg. This system is based on the observation of electromagnetic radiation or atomic emission spectra when samples are injected into an inductively coupled plasma atomization and excitation source. After the excitation of electron to excited state by plasma, electron must be back to the ground state and emit the unique emission spectra of a particular element, the amount of metal can be defined by the intensity of emission spectra. In Figure 2.7, a quartz tube approximately 2.5 cm diameter is taken inside a coil connected to a high frequency generator operating typically in the 4-50 MHz range at generator output level of 2-5 kW. When the generator power is turned on, the flowing Ar inside the tube will generate the plasma after a few popping flashes at the open end of the tube [54].
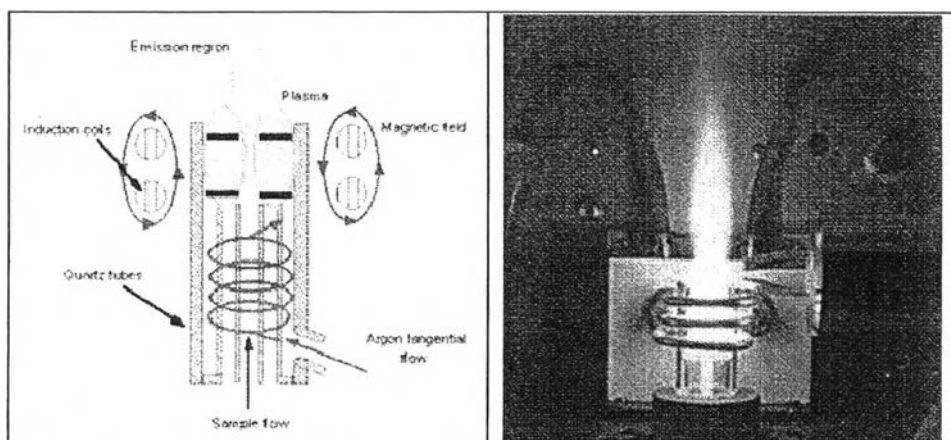

Figure 2.7 Plasma Torch [55]

2.7 Enhanced permeability and retention (EPR) effect

Enhanced permeability and retention (EPR) effect is the enhancement vascular permeability phenomenon, which tends to occur in tumor tissues much more than in normal tissues. The reason to generate this phenomenon is concerning with a quickly growing up of tumor tissues. They need an adequate supply to great demands of rapidly growing tumors such as nutrients and possibly oxygen, so that blood vessels must be regenerated, resulting in the leaky blood vessels in tumor cells as shown in figure 2.8. This phenomenon is well advantage for the delivery of macromolecular anticancer agents to selective tumor tissues [15-17, 56].
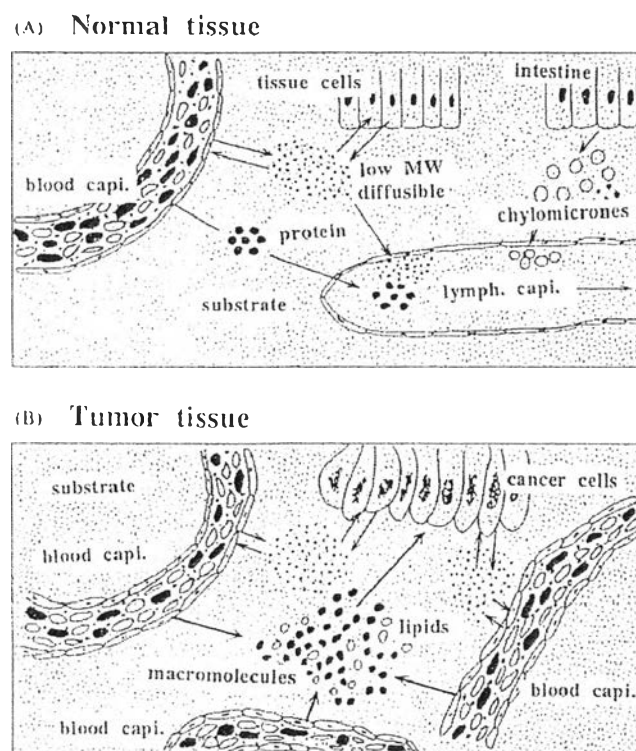

Figure 2.8 Schematic representation of differences in vascular anatomy of normal tissue (A) and tumor tissue (B). Note the excessive network development of vessels and extravasation of macromolecules and lipid particles in tumor [56].

2.8 Literature reviews

2.8.1 Literature reviews of difluoroboron complex of curcumin

Difluoroboron curcumin derivative, **CurBF₂** has been firstly reported to inhibit to the HIV-1 with the IC_{50} value of 24 μM [57]. Recently, Chaicham and co-workers [58] have reported the synthesis of the novel curcumin derivatives including, **CurBF₂**, **CurBF₂OTs** and **CurBF₂(OTs)₂**, which were used to study in the field of photophysical properties, and cyanide detection in aqueous solution. In Figure 2.9A, the deprotonation by a strongly basic anion at the hydroxyl group caused a large charge separation between acceptor and donor unit in **CurBF₂** resulting in a strong intramolecular charge transfer (ICT). The **CurBF₂** based the binding of CN⁻ complex could stabilize the exited states of complex which caused a bathochromic shift in the absorption band leading to the naked colorimetric changes from red to blue when the concentration of CN⁻ was increase from 0 to 57 mM (Figure 2.9B(a-i)).
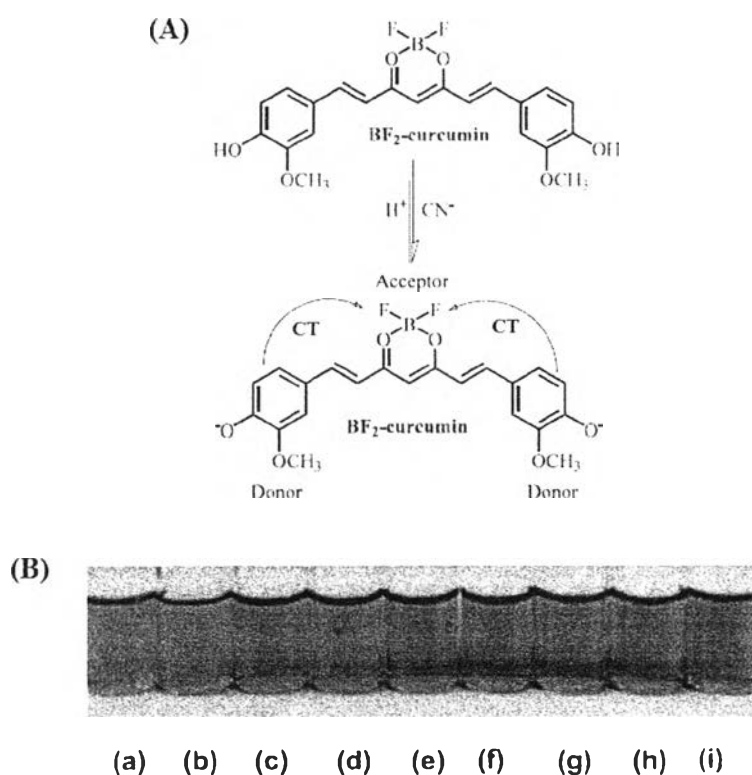

Figure 2.9 The ICT process (A) and colorimetric changes of **CurBF₂** (B) (0.01 mM) in CH_3CN/H_2O (4:1,v/v) upon the addition of (a) 0, (b) (15), (c) 22, (d) 24, (e) 29, (f) 36, (g) 43, (h) 50, and (i) 57 mM of CN⁻ [58]

2.8.2 Literature reviews of nanocarriers for delivery of curcumin to cancer cells

Anita and co-workers [7] have used O-carboxymethyl chitosan (O-CMC structure shown in Figure 2.10(A)) to encapsulate curcumin. From Figure 2.10(B) showed that curcumin was insoluble in water (a), in contrast the curcumin-O-CMC NPs could be clearly improved the water-solubility (c). Cellular uptake of curcumin-O-CMC NPs was monitored by fluorescence microscopy, which displayed the green channel defining the internalization of NPs in MCF-7 cancer cells (Figure 2.10(C)). The curcumin release was explained by the swelling property of O-CMC polymer. At the low pH as same as the pH of cancer cells, the residual amine was protonated to positive charge causing the repulsive force in the polymer matrix, thus leading to more drug was released. The cytotoxicity of curcumin-O-CMC NPs showed non-toxicity to the normal cell whereas the NPs showed the considerable toxicity to MCF-7 and PC-3 cancer cells and higher than the curcumin dissolved in DMSO (Figure 2.10(D-F)).
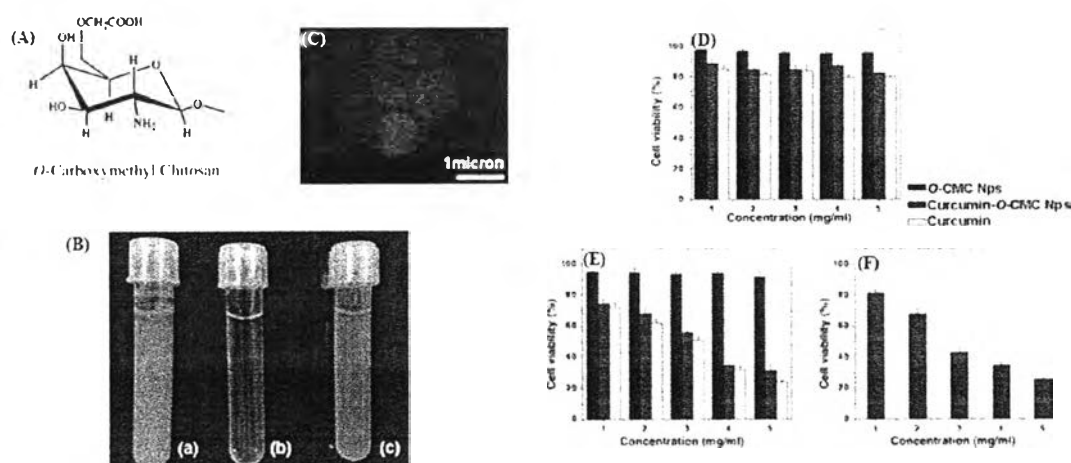

Figure 2.10 (A) Chemical structure of O-CMC. (B) Water-solubility of (a) curcumin (b) O-CMC Nps (c) curcumin-O-CMC Nps. (C) fluorescent image of MCF-7 at 100× of MCF-7 cancer cells treated with 5mg/ml curcumin-O-CMC Nps. (D) Cell viability of normal cells (L929) (E) breast cancer cells (MCF-7) and (F) prostate cancer cells (PC-3) treated with O-CMC Nps, curcumin and curcumin-O-CMC Nps [7].

Tang and co-workers [8] have prepared 8 types of polymercurcumins by condensation polymerization of curcumin. A polyacetal-based polycurcumin (PCurc8) was hydrolyzed and released active curcumin at the low pH and it showed highly cytotoxic to SKOV-3 cancers with IC_{50} value of 5.7 μg/mL, in term of its curcumin equivalent doses was IC_{50} value of 1.2 μg/mL. In acidic condition, the hydrolysis of PCurc8 at the acetal bonds could occur and produce the oligomers and curcumin as shown in Figure 2.11(a). The case of curcumin, dissolved in DMSO before a dilution in medium to the needed dose, exposed the cytotoxic to SKOV-3 cancers with IC_{50} value of 7.8 μg/mL (Figure 2.11(b)). It confirmed that the PCurc8 was more cytotoxic to cancer cell than curcumin based on the enhancement of water solubility and stability in physiological condition. Cellular uptake of PCurc8 by quickly endocytosis into the cells was monitored by confocal fluorescence at the incubation for 2 and 24 h as shown in Figure 2.11(c-d).
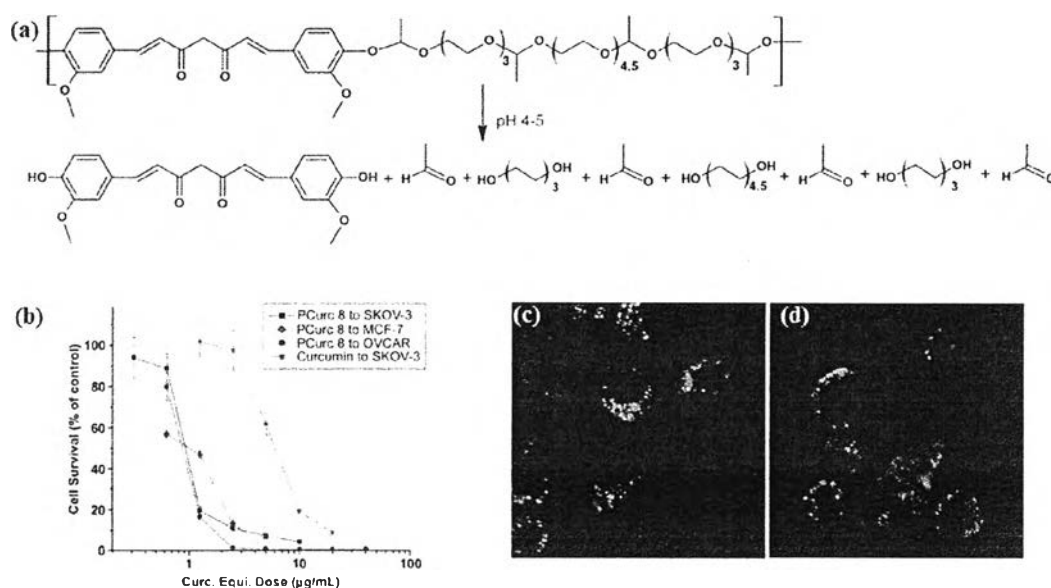

Figure 2.11 Acid catalyzed hydrolysis of PCurc8 (a). Cytotoxicities of PCurc8 compared with free curcumin to various cancer cell lines (b). Confocal fluorescence images of SKOV-3 cells were treated by PCurc8 for 2 (c) and 24 h (d) [8].

2.8.3 Literature reviews of lanthanide ion particles

Rill and co-workers [23] prepared neodymium, europium and ytterbium oxide/hydroxide colloids by water in oil microemulsion approach (Figure 2.12A). They study the effect of parameters preparation and precursors such as types of lanthanide ions and types of surfactants including positive charge SDS, negative charge CTAB and non-ionic surfactant Triton x-100 on the particles size and crytallinity. The structure of surfactants was shown in Figure 2.12B(a-c) and the TEM morphology of YbClSDS and NdClSDS were shown in Figure 2.12C(a-b). From the determination of particle size of the particles by using DLS technique shown in Figure 2.12D, it illustrated that the size distribution of particle from EuClSDS and YbClSDS were smaller than NdClSDS, which were possibly due to the stability in bivalent forms of Eu and Yb solutions. In the case of Nd solution, it could be stable in the trivalent form. For the surfactant study, Triton x-100 provided the size distribution smeller than CTAB and SDS. The possible reason would depend on the type of surfactants. The non-ionic Triton x-100 surfactant was well soluble in both separate water and oil phase and then, the formation of surfactant and lanthanide ions was immediately occurred. To obtain the clear microemulsion in the case of SDS, the sample should be continuously stirred for a long period time up to 2 h.
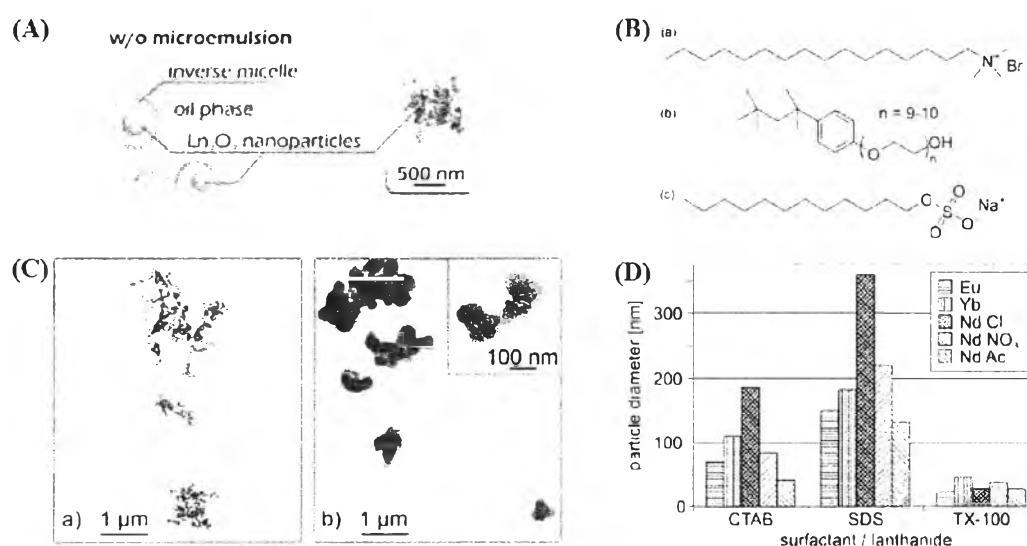

Figure 2.12 (A) schematic phase of water-oil microemulsion. (B) Chemical structure of CTAB, Triton x-100 and SDS. (C) TEM images of YbClSDS and NdClSDS. (D) Summarized particle size of samples determined by DLS [23].

Xiong and co-workers [10] created amine-functionalized rare-earth up-converting nanophosphors (UNPs) to use only as the luminescence imaging agent of tumors cells both *in vivo* and *in vitro* studies. The nanophosphors were prepared from lanthanide ions, AOT surfactant and 6-aminohexanoic acid by a modified hydrothermal microemulsion method as shown in Figure 2.13(A). The amine component not only assisted the water solubility, but also interacted with the folic acid (FA), and then the FA-coupled UCNPs were delivered into the cancer cells upon the folate-receptor protein (FR) overexpressing in various cancer cells. The up-converting nanophosphor morphologies with the particle size of 20-40 nm was shown in Figure 2.13(B). The *in vitro* cellular uptake of HeLa cancer cells were examined by up-conversion luminescence (UCL) of UCNPs. The UCL signals showed a green emission attributed to the $^2H_{11/2} \rightarrow {}^4I_{15/2}$ and $^4S_{3/2} \rightarrow {}^4I_{15/2}$ transitions and a red emission due to the transition the $^4F_{9/2} \rightarrow {}^4I_{15/2}$ of the Er^{3+}, which were shown in Figure 2.13(C-D), respectively. Moreover, UCNPs showed a significant UCL signal after intravenous injection in tumor cell as shown in Figure 2.13(E).
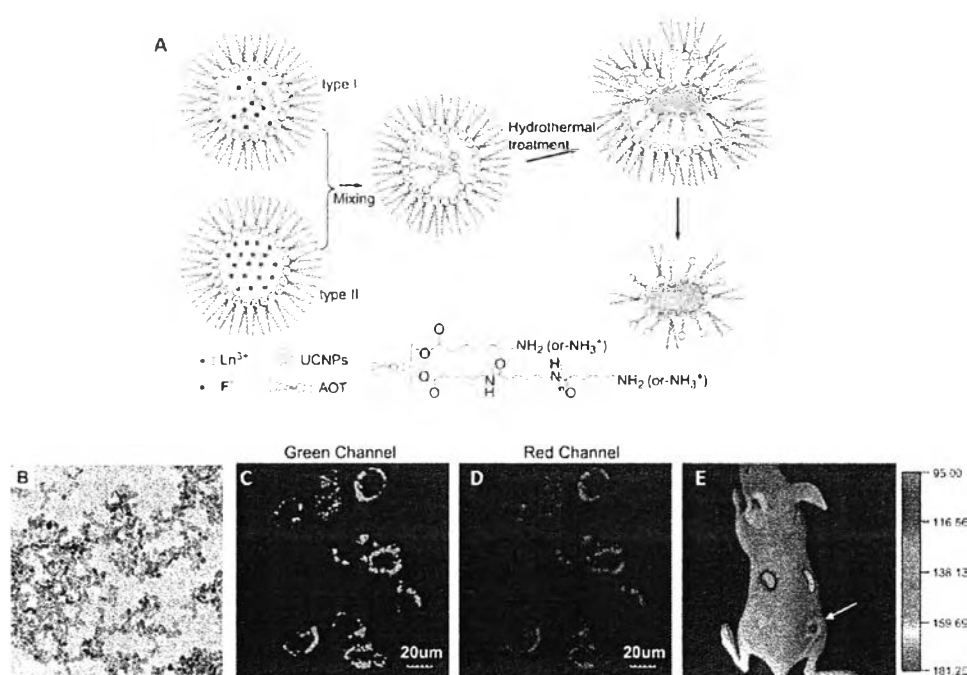

Figure 2.13 Synthesis of biocompatible UCNPs by a modified hydrothermal microemulsion route (A). HR-TEM images of NaYF4:Yb,Er samples (B). Green channel (C) and red channel confocal images (D) of HeLa cells incubated with UCNPs-FA by using LSUCLM with CW 980-nm laser. *In vivo* up-conversion luminescence imaging of subcutaneous HeLa tumor-bearing athymic nude mice (E) (pointed by white arrows) after intravenous injection of UCNPs-FA [10]

Nishiyabu and co-workers [19] reported the nanoparticles of nucleotide/lanthanide supramolecular networks in HEPES buffer solution pH 7.4 by the formation mechanism in Figure 2.14(a), which obtained the nanoparticles with diameter range of 30-179 nm as shown in Figure 2.14(b). The nanoparticles from various lanthanide ions and many nucleotides yielded the various excellent optical properties. For example, in Figure 2.14(c), the nanoparticles from GMP/Tb showed an enhancing the intensity of Tb^{3+} lanthanide luminescence by energy transfer from GMP nucleotide to Tb^{3+} ions. And the nanoparticles from 5'-GMP/Gd^{3+} exposed the excellent performance as a contrast agent for MR imaging as shown in Figure 2.14(d). It is a good candidate for using in biological imaging agent.
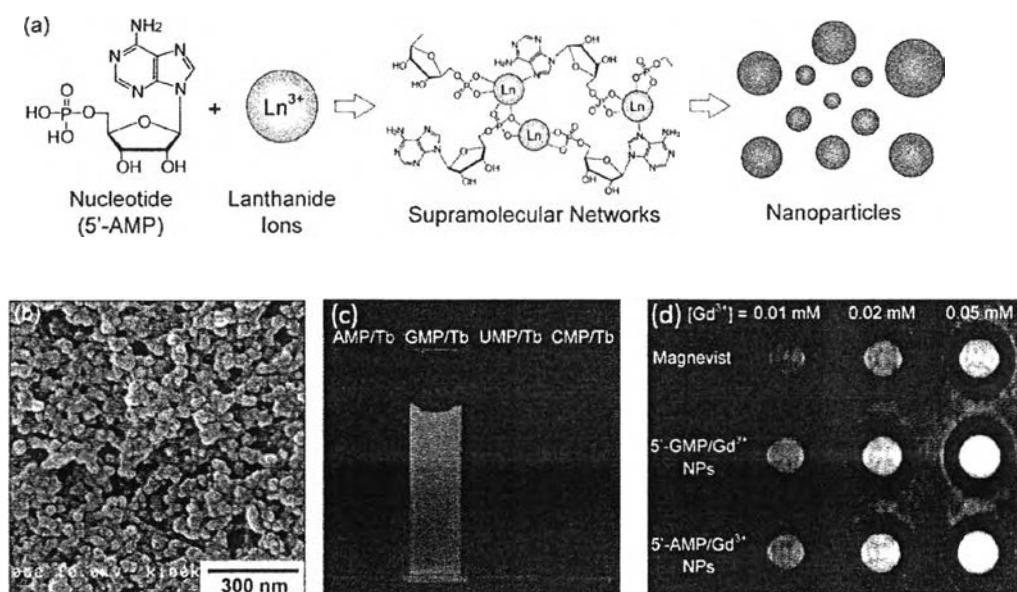

Figure 2.14 (a) A schematic illustration of nanoparticle formation through the self-assembly of 5'-AMP and Gd^{3+} ions in 0.1 M HEPES buffer. (b) SEM image of 5'-AMP/Gd^{3+} nanoparticles. (c) Luminescent and (d) MR imaging abilities of nucleotide/lanthanide nanoparticles [19].

Nucleotides were selected as a one of the precursor because they were biocompatible and exposed rich structural diversity. And lanthanide ions were also selected because they showed large coordination number, which may be form the flexible adaption with the size and shape of guest molecule. HEPES buffer solution was selected because it was wildly used in the biological research and showed the effective reducing agent to Au^{3+} ions providing Au nanoparticles and also exhibited surfactant ability when a concentration of HEPES > 10 mM [30]. The incorporation of dye molecules (Figure 2.15(a)) into 5'-AMP/Gd^{3+} nanoparticles by adaptive

supramolecular network self- assembly were obtained as shown in Figure 2.15(b). The result showed that the anionic dye molecules could incorporate into the nanoparticle more easily than the cationic dye molecules, and the dye doped nanopartcles showed intense luminescence even in the solid state based on the preventing the aggregation of dye molecules (Figure 2.15(c)). The adaptive dye encapsulation in suparmolecular networker via the coordination of lanthanides ions and carbonyl group or hydroxyl group of dye molecule was shown in Figure 2.15(d). These features provide a simple way to design multifunctional nanomaterials.
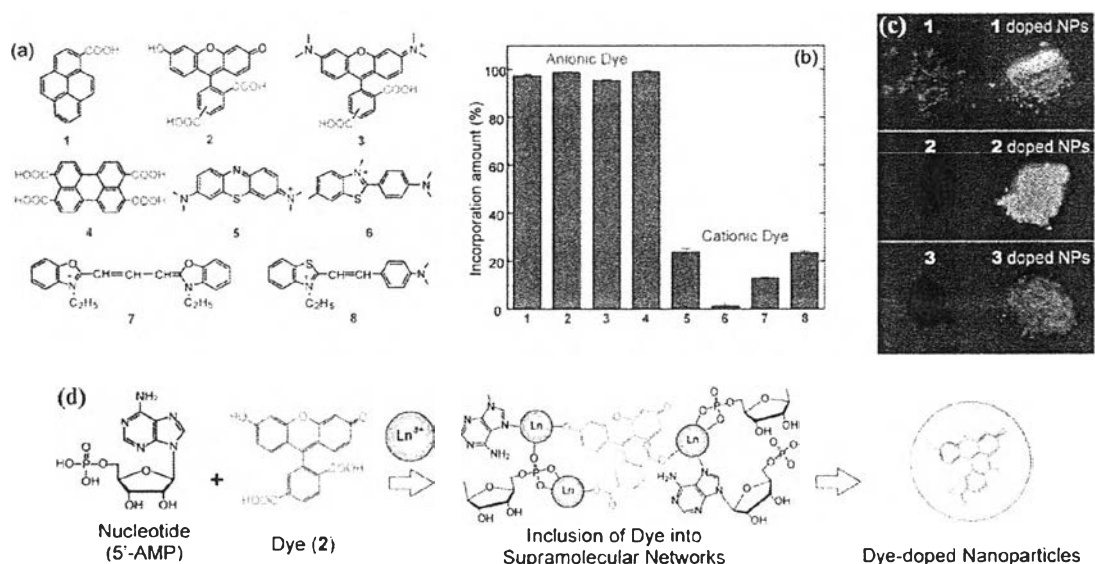

Figure 2.15 (a) Chemical structures of guest dyes. (b) Binding ratio (%) of various dyes to 5'-AMP/Gd^{3+} NPs. (c) Photographs of powder samples of solid dyes **1, 2,** and **3** (left) and **1, 2,** and **3**-doped 5'-AMP/Lu^{3+} nanoparticles (right). Samples were illuminated by the 365 nm UV light. (d) Schematic illustration of adaptive dye encapsulation in supramolecular networks [19].

2.9 Hypothesis of this research

From the previous research, Rill and co-workers [23] have reported the colloids from lanthanide oxide/hydroxide and surfactants by water in oil microemulsion approach. Then, Rui and co-workers [59] have reported the flocculation of lanthanide (III) metal ions by SDS surfactant in aqueous solution. These materials showed water-insoluble reverse-microemulsion structure. The research of Nishiyabu and co-workers [19] utilized the nanoparticles of adaptive supramolecular networks self-assembly in HEPES buffer solution pH 7.4 from nucleotides and lanthanide ions for increasing the intensity of fluorescent dyes and for applying to biomedical materials. Likewise, Kulchat and co-workers [20] also used those coordination nanoparticles to stabilize the boronic acid/ fluorescein sensors for detection of cyanide ions in HEPES buffer solution.

In this research, we expect to prepare the novel nanoparticles from gadolinium (III) ions and surfactants in 0.1 M HEPES buffer solution pH 7.4, which is an easy method, and the surfactants are cheaper than the nucleotides. The adaptive dye encapsulated in supramolecular networks will be obtained by self-assembly of Gd^{3+} based and surfactants in HEPES buffer. Moreover, when the concentration of HEPES was more than 10 mM, it would exhibit the surfactant activity. Sulfate and hydroxyl groups in the molecular structure of HEPES buffer not only assist the formation of nanoparticles, but also increase the water-solubility of nanoparticles. We hypothesize that the stable drug-doped nanoparticles with the suitable particle size are delivered pass through the leaky tumor blood vessels of the target tumor by EPR effect and expressed the anti-cancer activity of drug to cancer cells. Moreover, these materials based Gd^{3+} would be applied as further contrast agent for magnetic resonance image (MRI).